Simulating the formation of carbonaceous aerosol in a European Megacity (Paris) during the MEGAPOLI summer and winter campaigns

C. Fountoukis[1], A.G. Megaritis[2], K. Skyllakou[2], P.E. Charalampidis[1,3], H.A.C. Denier van der Gon[4], M. Crippa[5,6], A. S. H. Prévôt[6], F. Freutel[7], A. Wiedensohler[8], C. Pilinis[3] and S.N. Pandis[1,2,9,*]

[1] Institute of Chemical Engineering Sciences, Foundation for Research and Technology Hellas (FORTH), 26504 Patras, Greece
[2] Department of Chemical Engineering, University of Patras, 26500 Patras, Greece
[3] Department of Environment, University of the Aegean, 81100 Mytilene, Greece
[4] TNO Climate, Air and Sustainability, PO Box 80015, 3508 TA Utrecht, The Netherlands
[5] EC Joint Research Centre (JRC), Inst. Environment & Sustainability, Via Fermi, Ispra, Italy
[6] Laboratory of Atmospheric Chemistry, Paul Scherrer Institute, PSI Villigen, Switzerland
[7] Max Planck Institute for Chemistry, Particle Chemistry Department, Mainz, Germany
[8] Leibniz Institute for Tropospheric Research, Leipzig, Germany
[9] Department of Chemical Engineering, Carnegie Mellon University, Pittsburgh, USA

*Correspondence to: Spyros N. Pandis (Chemical Engineering Department, University of Patras, Patra, GR-26500, Greece, email: spyros@chemeng.upatras.gr, Tel: +30 2610 969510, Fax: +30 2610 969713)

Abstract

We use a three dimensional regional chemical transport model (PMCAMx) with high grid resolution and high resolution emissions (4 × 4 km^2) over the Paris greater area to simulate the formation of carbonaceous aerosol during a summer (July 2009) and a winter (January/February 2010) period as part of the MEGAPOLI (Megacities: Emissions, urban, regional, and Global Atmospheric POLlution and climate effects, and Integrated tools for assessment and mitigation) campaigns. Model predictions of carbonaceous aerosol are compared against Aerodyne aerosol mass spectrometer and black carbon (BC) high time resolution measurements from three ground sites. PMCAMx predicts BC concentrations reasonably well reproducing the majority (70%) of the hourly data within a factor of two during both periods. The agreement for the summertime secondary organic aerosol (OA) concentrations is also encouraging (mean bias = 0.1 μg m^{-3}) during a photochemically intense period. The model tends to underpredict the summertime primary OA concentrations in the Paris greater area (by approximately 0.8 μg m^{-3}) mainly due to missing primary OA emissions from cooking activities. The total cooking emissions are estimated to be approximately 80 mg d^{-1} per capita and have a distinct diurnal profile in which 50% of the daily cooking OA is emitted during lunch time (12:00 – 14:00 LT) and 20% during dinner time (20:00-22:00 LT). Results also show a large underestimation of secondary OA in the Paris greater area during wintertime (mean bias = -2.3 μg m^{-3}) pointing towards a secondary OA formation process during low photochemical activity periods that is not simulated in the model.

1 Introduction

Megacities (cities with more than 10 million inhabitants) are major sources of gas and particulate pollutants affecting public health, regional ecosystems, and climate. Rapid urbanization requires efficient emission control strategies and cost-effective air quality management. One of the main challenges in the design of abatement strategies for large urban agglomerations is the quantification of the contributions of local and long-range pollutant transport as well as the identification of the emission areas affecting the receptor. Ambient fine particulate matter ($PM_{2.5}$) is one of the main targets of such pollution reduction strategies. Organic aerosol makes up a large part of $PM_{2.5}$ but despite its importance, it remains the least understood component of the atmospheric aerosol system. Understanding the formation and sources of organic aerosol in megacities is a critical step towards developing efficient mitigation strategies.

Intensive field measurement campaigns have been performed to characterize the chemical composition of particulate and gaseous pollutants in megacities such as New York (Sun et al., 2011), the Los Angeles basin (Hersey et al., 2011), Mexico City (Molina et al., 2010), London (Allan et al., 2010), Tokyo (Xing et al., 2011), and Beijing (Sun et al., 2010). In Europe comprehensive atmospheric measurements were recently conducted in the Paris metropolitan area as part of the MEGAPOLI project (Crippa et al., 2013a,b,c; Freutel et al., 2013; Freney et al., 2013). Freutel et al. (2013) analyzed aerosol mass spectrometer (AMS) measurements from 3 stationary sites in the Paris area during July 2009. They found that the origin of air masses had a large influence on secondary (oxygenated) organic aerosol (OOA) concentrations with elevated values (up to 7 $\mu g\ m^{-3}$) observed during periods when the site was affected by transport from continental Europe and lower concentrations (1 - 3 $\mu g\ m^{-3}$) when air masses were originating from the Atlantic. Crippa et al. (2013a) used positive

matrix factorization (PMF) to perform organic source apportionment during winter 2010 in Paris. They identified three dominant primary sources (traffic: 11–15% of OA, biomass burning: 13–15% and cooking up to 35% during meal hours). Oxygenated OA was found to contribute more than 50% to the total OA and included a highly oxidized factor and a less oxidized factor related to aged wood burning emissions. Crippa et al. (2013b) focused on secondary OA (SOA) during both winter and summer in Paris and showed that OOA (local semi-volatile OOA (SV-OOA) and regional low-volatility OOA (LV-OOA)) was significant during both seasons (24–50% of total OA), while contributions from photochemistry-driven OOA (daytime SV-OOA) (9% of total OA) and aged marine OA (13% of total OA) were also observed during summertime. A semivolatile nighttime OOA factor correlating with nitrate was also identified representing 2% of total OA during summer and 18% in winter. Freney et al. (2014) analyzed airborne AMS measurements during summer and found that OA increased with photochemical aging demonstrating that it is necessary to take into account a continental-scale geographical area (compared to a local/city-scale area) when assessing the formation of SOA from urban emissions.

Organic aerosol has hundreds of sources, both anthropogenic and natural, in both the particulate and gas phases, while it can undergo complex atmospheric chemical and physical processing (Hallquist et al., 2009). The description of all these emissions and processes in Chemical Transport Models (CTMs) is not a trivial task. Earlier modeling efforts for the megacity of Paris (Sciare et al., 2010) have assumed that primary OA (POA) is non-volatile and used a single-step oxidation SOA scheme thus underestimating SOA concentrations by a factor of three. Even larger errors were encountered when aged air masses with high SOA levels arrived at the observation site. More recently, models taking into account the semivolatile nature of POA (Robinson et al., 2007) have been applied over Paris. Couvidat et

al. (2013) applied the Polyphemus model, which incorporates a two-surrogate-species (hydrophilic/hydrophobic) SOA formation scheme taking into account POA volatility and chemical aging, during the MEGAPOLI July 2009 campaign. The model estimated a 30 - 38% local contribution to OA at the city center and overpredicted morning OC concentrations. Zhang et al. (2013) implemented the volatility basis set (VBS) approach into the chemistry transport model CHIMERE and applied it to the greater Paris region for the summer MEGAPOLI campaign. Simulation of organic aerosol with the VBS approach showed the best correlation with measurements compared to other modeling approaches. They also showed that advection of SOA from outside Paris was mostly responsible for the highest OA concentration levels. Fountoukis et al. (2013) examined the role of horizontal grid resolution on the performance of the regional 3-D CTM PMCAMx over the Paris greater area during both summer and winter and concluded that the major reasons for the discrepancies between the model predictions and observations in both seasons are not due to the grid scale used, but to other problems (e.g., emissions and/or process description). Skyllakou et al. (2014), using the Particulate Matter Source Apportionment Technology (PSAT) together with PMCAMx, showed that approximately 50% of the predicted fresh POA originated from local sources and another 45% from areas 100–500 km away from the receptor region during summer in Paris. Furthermore they found that more than 45% of OOA was due to the oxidation of volatile organic compounds (VOCs) that were emitted 100 - 500 km away from the center of Paris.

Although several uncertainties still exist in OA modeling (e.g. related to POA volatility, SOA yields, the aging parameterization), evaluation and improvement of emission inventories from megacities as well as from surrounding areas is of fundamental importance. Furthermore, the description of the subsequent aging of the emitted organic material and the

137 formation of OOA is critical in OA modeling. In this work we use the 3-D regional CTM
138 PMCAMx with fine grid resolution to evaluate the OA and BC emission inventory in the
139 megacity of Paris. We use an extensive set of factor analysis AMS data which allow a more
140 in-depth evaluation of the formation and evolution of OA. We identify and quantify missing
141 sources of OA during both seasons, explore possible emission and meteorological errors
142 affecting the predicted BC concentrations and discuss missing or inadequate processes
143 forming OA in the model.
144
145 **2 Model description**
146 PMCAMx (Tsimpidi et al., 2010; Fountoukis et al., 2011, 2014b) describes the
147 processes of horizontal and vertical transport, gas-and aqueous-phase chemistry, aerosol
148 dynamics and chemistry, and wet and dry deposition. It is based on the framework of the
149 CAMx air quality model (Environ, 2003). An extended SAPRC99 mechanism (Environ,
150 2003) is used in the gas-phase chemistry module. The OA treatment in PMCAMx is based on
151 the Volatility Basis Set (VBS) approach (Donahue et al., 2006; 2009) for both primary and
152 secondary organic species. Primary OA is assumed to be semivolatile with nine surrogate
153 POA species used, corresponding to nine effective saturation concentrations ranging from 10^{-2}
154 to 10^{6} μg m^{-3} (at 298 K) in logarithmically spaced bins (Shrivastava et al., 2008). POA is
155 simulated in the model as fresh (unoxidized) POA and oxidized POA from i) intermediate
156 volatility organic compounds (IVOCs) and ii) semi-volatile organic compounds (SVOCs)
157 (SOA-iv and SOA-sv, respectively). The IVOCs emissions are assumed to be proportional
158 (by a factor of 1.5) to the emitted primary OA mass (Tsimpidi et al., 2010; Shrivastava et al.,
159 2008). The SOA volatility basis-set approach (Lane et al., 2008) of the model includes four
160 SOA species for each VOC with four volatility bins (1, 10, 100, 1000 μg m^{-3}). Chemical

aging is modeled through gas-phase oxidation of OA vapors using a gas-phase OH reaction with a rate constant of 1×10^{-11} cm^3 $molec^{-1}$ s^{-1} for SOA from anthropogenic VOCs (aSOA-v) and 4×10^{-11} cm^3 $molec^{-1}$ s^{-1} for SOA-sv and SOA-iv (Atkinson and Arey, 2003). Each reaction is assumed to decrease the volatility of the vapor material by one order of magnitude. More details about this version of the model can be found in Fountoukis et al. (2011; 2014b).

The parameterization of the biogenic SOA chemical aging in the VBS scheme in this work differs from that used by Zhang et al. (2013) in CHIMERE. In CHIMERE the biogenic SOA ages the same way as the anthropogenic SOA, while in our work these later generation reactions are assumed to lead to a zero net increase of the corresponding SOA because of a balance between the functionalization and fragmentation processes.

3 Model application

We simulate two periods (1 – 30 July 2009 and 10 January – 9 February 2010) during which intensive measurement campaigns were performed as part of MEGAPOLI. PMCAMx is used with a two-way nested grid structure which allows the model to run with coarse grid spacing over the regional domain of Europe, while within the same simulation, applying a fine grid nest over the Paris greater area (Fig. 1). The necessary meteorological inputs to the model were generated from the WRF (Weather Research and Forecasting) model (Skamarock et al., 2008) and include horizontal wind components, vertical diffusivity, temperature, pressure, water vapor, clouds and rainfall. WRF was driven by static geographical and dynamic meteorological data (near real-time and historical data generated by the Global Forecast System (1×1°)). 27 sigma-p layers up to 0.1 bars were used in the vertical dimension. Each layer of PMCAMx was aligned with the layers used in WRF. PMCAMx was set to perform simulations on a polar stereographic map projection with 36×36 km^2 grid

185 spacing over the European domain and a 4 × 4 km^2 resolution over Paris. The European
186 modeling domain covers a 5400 × 5832 km^2 region while the Paris subdomain covers a total
187 area of 216 × 180 km^2 with the Metropolitan area of Paris located centrally in the subdomain.
188 Fourteen vertical layers are used extending up to 6 km in height with a surface layer depth of
189 55 m. The dimensions of the modeling domain are the same for both the summer and winter
190 simulations. The model interpolates the meteorological input from the parent to the nested
191 grid while high resolution emissions are used in the Paris subdomain. Concentrations of
192 species at the boundaries of the domain are based on measured average background
193 concentrations in sites close to the boundaries of the domain (e.g. Zhang et al., 2007; Seinfeld
194 and Pandis 2006). We have used the same boundary conditions as in Fountoukis et al. (2011).
195 Inventories of both biogenic and anthropogenic emissions were developed and consist
196 of hourly gridded emissions of gases as well as primary particulate matter. A description of
197 the European emission data can be found in Pouliot et al. (2012). These emissions were
198 modified by nesting high resolution emissions with emission inventories for four megacities
199 in the European coarser grid of 36×36 km^2. More specifically, the base case emission data
200 originate from the Netherlands Organization for Applied Scientific Research (TNO) and were
201 compiled as part of the MEGAPOLI project. They were spatially distributed at a resolution of
202 1/8° × 1/16° (longitude × latitude). Furthermore, based on the TNO inventory, bottom-up
203 emission data were used for four European megacities (Paris, London, Rhine-Ruhr and Po
204 Valley). A description of the procedure for the nesting, comparison and origin of the different
205 emission inventories is given in Kuenen et al. (2010) and Denier van der Gon et al. (2011).
206 The Paris emissions that form the core of the high resolution inventory for the domain
207 used in this study originate from local authorities responsible for city emissions inventories
208 and air quality (Airparif, 2010). A summary of total mass emission rates for the Paris greater

209 area is given in Table 1. The largest source of primary OA in the wintertime emission
210 inventory in Paris is residential (wood and fossil fuel) combustion, contributing 80% to the
211 total anthropogenic OA emissions while during summer the traffic-related sector dominates
212 with 35% contribution (Table S1). During winter the traffic sector contributes approximately
213 40% to the total BC emissions in the Paris subdomain. This is more than a factor of two
214 higher than the European average contribution and is due to the dense population in this area.
215 The residential combustion sector contributes approximately 45% to the wintertime BC
216 emissions in the Paris area which is about the same as the European average indicating low
217 emissions per inhabitant in the Paris greater area for this specific source sector.

218 The chemical speciation of the volatile organic compounds is based on the speciation
219 approach proposed by Visschedijk et al. (2007). Biogenic emissions were estimated using
220 three distinct inventories. Plant canopy gridded emissions were estimated by utilizing the
221 MEGAN (Model of Emissions of Gases and Aerosols from Nature) model (Guenther et al.,
222 2006). MEGAN inputs are meteorological parameters estimated by the WRF model, the leaf
223 area index and a set of emission factors for various chemical species at standard conditions.
224 Since a large portion of the domain is covered by sea, marine aerosol emissions are also
225 included. These are based on a marine aerosol model (O'Dowd et al., 2008) that estimates
226 mass fluxes for both accumulation and coarse mode including an organic fine mode aerosol
227 fraction. Inputs of the specific marine model are the wind speed components calculated by
228 WRF and the chlorophyll-a concentrations acquired using the GES-DISC Interactive Online
229 Visualization ANd aNalysis Infrastructure (GIOVANNI) as part of the NASA's Goddard
230 Earth Sciences (GES) Data and Information Services Center (DISC). Finally wildfire
231 emissions are also included (Sofiev et al., 2009).
232

4 Measurements

Two intensive field campaigns were performed as part of the MEGAPOLI project (megapoli.dmi.dk/index.html) during summer (July 2009) and winter (January/February 2010) in the Paris area including AMS measurements of fine particulate matter from three ground sites (Beekmann et al., 2014). The Laboratoire d'Hygiène de la Ville de Paris (LHVP; Paris, 13th district; 48.827 N, 2.358 E) monitoring station is in the center of the city and is representative of Paris urban background air pollution (Sciare et al., 2010; Favez et al., 2007). SIRTA (Site Instrumental de Recherche par Télédétection Atmosphérique) is located in Palaiseau (48.714 N, 2.203 E), 20 km south-west of the city center and is characteristic of a suburban environment (Haeffelin et al., 2005). The GOLF (GOLF Poudrière) site (48.934 N, 2.547 E) is located approximately 20 km to the north east of the city center and is also suburban influenced by local (medium) traffic. High-resolution time-of-flight aerosol mass spectrometers (HR-ToF-AMS) (DeCarlo et al., 2006) were used at both the SIRTA and LHVP sites, while a compact ToF-AMS (C-ToF-AMS) (Drewnick et al., 2005) was deployed at GOLF. AMS OA measurements were analyzed by factor analysis (Crippa et al., 2013b) using the multi-linear engine (ME-2) algorithm (Paatero, 1999; Canonaco et al., 2013), the PMF2 algorithm (Freutel et al., 2013) and the PET toolkit of Ulbrich et al. (2009) (Crippa et al., 2013a,c). The factor analysis data used in this work are taken from Crippa et al. (2013b) for LHVP, from Crippa et al. (2013c) for SIRTA and from Freutel et al. (2013) for the GOLF site during the summer period while during winter all the data are taken from Crippa et al. (2013a). Table 2 shows the various OA components identified by the PMF analysis in each site and season. During the winter campaign factor analysis identified two primary OA components (hydrocarbon-like organic aerosol (HOA) and biomass burning OA (BBOA)) in GOLF with the addition of cooking-related organic aerosol (COA) component in LHVP and

SIRTA. Two secondary components (low-volatility OOA related to wood burning emissions and a highly oxidized OOA factor) were identified in LHVP and GOLF and one OOA component in SIRTA. During summertime two primary OA components (COA and HOA) were identified in LHVP and SIRTA and one component (HOA) at GOLF. Finally, one OOA component was identified in GOLF, while three (marine-related OA, (MOA), low-volatility oxygenated OA (LV-OOA) and semi-volatile oxygenated OA (SV-OOA)) were identified at SIRTA and LHVP. BC was measured using a multi-angle absorption photometer (MAAP) in LHVP and GOLF and an Aethalometer in SIRTA (Freutel et al., 2013). The measurement uncertainty for the aethalometer and MAAP was 30% and 10%, respectively (Freutel et al., 2013).

5 Results and discussion

5.1 Model predictions over the Paris greater area

Figure 2 shows the predicted average ground-level concentrations of fine fresh primary OA, secondary OA and BC in the greater Paris area during July 2009 and January/February 2010. Overall, carbonaceous aerosol is predicted to account for 36% of total dry PM_1 mass concentration at ground level averaged over the Paris greater area domain during summer, followed by nitrate (20%), sulfate (16%) and ammonium (12%) with the remaining 16% comprised of crustal material, sea-salt and metal oxides. During the winter period the model predicts a higher contribution of carbonaceous aerosol (41%) and lower contributions for the secondary species: sulfate (12%), nitrate (12%) and ammonium (11%). Primary OA and BC are predicted to have higher levels in the city center while their concentrations decrease in the Parisian suburbs. The use of high resolution in both the emissions and grid simulation results in larger spatial concentration gradients compared to the resolution of 36×36 km^2 used by

Fountoukis et al. (2013). During the winter period the model predicts much higher concentrations for both POA and BC compared to summer. Based on the PSAT results, the two largest sources of primary carbonaceous aerosol are the traffic-related sector and the residential (fuel and wood) combustion processes. The traffic source sector dominates in the contribution of the OA and BC emissions during summer while during wintertime the residential combustion is the largest contributor.

Secondary OA concentrations show a regional character in their geographical distribution during both seasons with higher concentrations predicted during summer due to stronger photochemical activity. A west to east gradient is predicted during summer following the evolution of photochemistry. OOA is predicted to account for approximately 90% of PM_1 OA at ground level over the Paris greater area (domain-average) during summer and 50% during winter..

5.2 Primary organic aerosol levels and sources

The prediction skill metrics of PMCAMx against factor-analysis AMS data for total POA concentrations from all three stations in the Paris greater area are summarized in Table 3. Figure 3 shows an overall comparison of modeled versus observed values for both seasons. Primary OA in the model is the OA that is emitted in the particulate phase and has not undergone any chemical processing. The AMS total POA component in this comparison is the sum of HOA and COA during summer with the addition of BBOA during wintertime. During the summer period the model underpredicts total POA concentrations at all sites by, on average, 0.8 μg m^{-3}. Overall, only 15% of the hourly data from all sites (1700 data points in total) are predicted within a factor of two. At LHVP the agreement is slightly better but still poor, with 30% of the data predicted within a factor of two and a fractional error of 0.9.

305 The day-to-day variability of modeled and observed concentrations in Paris center is shown
306 in Fig. S1 in the supplement. The daily-average total POA concentration is systematically
307 underpredicted throughout most of the simulated days.

308 Factor analysis of the AMS data from downtown Paris showed that a major part (more
309 than 70%) of observed total POA concentrations originated from cooking activities (0.5 μg
310 m^{-3} on average) while only another 0.2 μg m^{-3} was attributed to HOA from traffic-related
311 sources (Crippa et al., 2013b). Emissions from cooking sources are not included in the
312 baseline emission inventories that are used in this work (Denier van der Gon et al., 2011).
313 Therefore any POA concentrations that the model predicts during the summer period are
314 mainly primary OA from traffic-related sources. This is further explored in Section 5.5.

315 During summer the model predicts low concentrations of vehicular POA in Paris,
316 ranging on average between 0.2 and 0.3 μg m^{-3}, in agreement with the observations (Fig. S2).
317 There is little bias (FBIAS=0.1) and the mean error is 0.2 μg m^{-3} (Table S2). In SIRTA the
318 predicted average diurnal profile compares well with the observations capturing the morning
319 peak at 8 am. The nocturnal bias in SIRTA (at 10 pm) is rather episodic with two days (4 and
320 11 July) exhibiting a large vehicular-POA underprediction (by more than a factor of 5).
321 Interestingly, observations show no clear morning peak at the city center. The model,
322 however, predicts a distinct diurnal profile, overpredicting vehicular POA concentrations at
323 LHVP during the morning rush hours. This overprediction of POA-traffic concentrations
324 could be related to emissions (e.g. emission rate errors, errors in the diurnal cycle of
325 emissions, missing sources of total POA emissions, etc.), errors in the geographical
326 distribution of emissions in the high resolution domain (Fountoukis et al., 2013) or could also
327 be affected by errors in the meteorology. The source apportionment method can also induce

328 errors. As HOA concentrations are quite low, the HOA fraction estimated by the statistical
329 model has large uncertainty (30-50%).

330 Meteorological parameters used as input to PMCAMx (temperature, relative humidity
331 and wind velocity) were compared against measurements available at SIRTA (Fig. S3). In
332 general, the WRF calculated meteorological fields are consistent with the measurements.
333 Temperature is well reproduced with a mean bias of -0.7 °C. There are a few days where
334 WRF underpredicts the maximum daily observed temperature by 2-4 °C which could
335 theoretically result in an underestimation of POA evaporation and thus a small overprediction
336 of POA. However, no correlation between the temperature errors and the POA or OOA bias
337 was found. No systematic error is found in the wind velocity or relative humidity comparison
338 (mean bias of 0.2 m s^{-1} and -0.5%, respectively).

339 During winter the agreement for total POA is better than in summer, with errors mostly
340 due to scatter (mean error = 1.4 μg m^{-3}) but also a tendency towards underprediction (mean
341 bias = -0.4 μg m^{-3}) (Fig. S1). Factor analysis of the AMS data from the city center showed an
342 average of 1 μg m^{-3} from cooking sources, 1 μg m^{-3} from biomass burning and 0.7 μg m^{-3}
343 from traffic (Crippa et al., 2013a). The model predicts an average of 2.2 μg m^{-3} for total POA
344 which includes both vehicular POA and BBOA but no COA concentrations. Source
345 apportionment results from Paris (Skyllakou et al., 2014) showed that approximately 70% of
346 the modeled (PMCAMx) total POA concentration in Paris center is predicted to originate
347 from biomass burning and 15% from traffic-related sources. This shows that the model
348 underpredicts the concentrations of POA-traffic components during winter (Table S2) while
349 the problem with the missing COA emissions still exists but is now a smaller fraction of the
350 total POA. The comparison between the predicted BBOA concentrations from PSAT against
351 the factor analysis BBOA (Fig. S4, Table S3) shows an overprediction in LHVP (mean bias =

352 0.3 μg m^{-3}) and underprediction at SIRTA (mean bias = -0.3 μg m^{-3}) implying errors in the
353 geographical distribution of residential wood burning emissions in the Paris greater area.
354
355 **5.3 Oxygenated organic aerosol**
356 Figure 4 shows the comparison of predicted OOA concentrations against the factor-
357 analysis AMS data for both seasons with the statistics of the comparison summarized in
358 Table 3. The modeled OOA is defined as the sum of aSOA-v, bSOA-v (SOA from biogenic
359 VOCs), SOA-iv and SOA-sv. Contrary to POA, the comparison for OOA during the summer
360 period is encouraging (Fig. S1). The model predicts an average of 1.5 μg m^{-3} of OOA at the
361 three measurement sites without any significant concentration gradients between the city
362 center (LHVP) and the suburban sites (Table 3) while a 1.4 μg m^{-3} average concentration was
363 estimated by the factor analysis. A large fraction (54%) of the predicted OOA concentration
364 in LHVP is bSOA-v followed by SOA-sv and SOA-iv (33%) and aSOA-v (13%). Most of the
365 OOA hourly measurements are reproduced within a factor of two (80% in both LHVP and
366 GOLF and 60% in SIRTA) highlighting the ability of the model to reproduce the major
367 secondary OA transport and transformation processes during a photochemically intense
368 period. This was also shown by Zhang et al. (2013) when using the VBS scheme as opposed
369 to the single-step SOA formation mechanism in LHVP during summertime. However, in
370 disagreement with this work, the VBS scheme assuming increasing biogenic SOA yields with
371 chemical aging of Zhang et al. (2013) systematically overpredicts OOA concentrations in the
372 city center (by up to a factor of two). PMCAMx reproduces the observed OOA
373 concentrations in LHVP during summer with reasonable accuracy (1.7 μg m^{-3} compared to
374 1.6 μg m^{-3} predicted by the model with a -0.05 fractional bias).

375 During the winter period however, the model performance is very different than in July.
376 PMCAMx largely underpredicts OOA concentrations at all three sites with an overall mean
377 bias of -2.3 μg m^{-3} (Table 3). It is noteworthy though that the OOA levels estimated by the
378 PMF analysis during the winter period are more than a factor of two higher than that of the
379 summer period. PMCAMx on the other hand predicts that OOA during winter is 30-50%
380 lower than during summer. Only 25% of the hourly data (2230 in total) are predicted within a
381 factor of two. The model predicts less than 1 μg m^{-3} of OOA in the Paris greater area while
382 the factor-analysis estimated a concentration of more than 3 μg m^{-3}. The OOA
383 underprediction is persistent throughout the simulation period (Fig. S5). However, there are
384 certain days with large (a factor of 3-5) underestimation (24 and 27 January and 4 and 7
385 February) and a couple of other days during which the model performance is somewhat
386 reasonable at least during certain hours of the day (29 January and 3 February). A back-
387 trajectory analysis (Fig. S6) shows that during the days with the larger underestimation, air
388 masses originated from continental Europe, either within France or from the northeast
389 (mostly Germany). while during the days with reasonable model performance the air masses
390 were mostly clean coming from the Atlantic. Possible reasons for this underprediction
391 include errors in meteorology, emission rate errors of SOA precursors and missing or
392 inadequate processes forming OOA in the model. However, no significant errors in the
393 wintertime meteorological input were found from the evaluation of the meteorological
394 parameters (Fig. S3). Furthermore, PMCAMx was found to perform reasonably well for other
395 PM components (e.g. BC) indicating that the meteorology is probably not the main reason for
396 the OOA underprediction. Simulations with PSAT together with PMCAMx showed that
397 approximately 80% of the predicted OOA during winter in Paris originated from long range
398 transport from areas more than 500 km away from Paris. Compared to summer (45%), the

399 model simulates more contribution from long range secondary OA sources during winter,
400 because the timescale for its production is longer due to the slower photochemical activity
401 (Skyllakou et al., 2014). Therefore any emission rate errors in OOA precursors, if true,
402 should be present not only in the Paris greater area but also in the greater region of Europe. In
403 fact recent studies (Bergstrom et al., 2012; Kostenidou et al., 2013; Fountoukis et al., 2014;
404 Denier van der Gon et al., 2014) have pointed towards large uncertainties in the biomass
405 burning emission estimates in many European areas. This could partly explain the wintertime
406 underprediction of OOA in Paris. If BBOA emissions are significantly underestimated in
407 European regions upwind of Paris, then the Parisian SOA-sv and SOA-iv concentrations
408 formed in the model from BBOA would also be underestimated. From the factor analysis of
409 Crippa et al., (2013b), an average of 1.3 μg m^{-3} was estimated for the oxygenated BBOA
410 (OBBOA) concentration in Paris, significantly higher compared to the OBBOA predictions
411 of PSAT (0.2 μg m^{-3}). However, this can explain only part of the large underprediction of
412 OOA (-2.3 μg m^{-3}). Some recent studies have supported the transformation of BBOA to OOA
413 without the presence of sunlight (Bougiatioti et al., 2013; Crippa et al., 2013a,b). A process
414 forming SOA (and involving high NO_x levels from polluted sites) that is not simulated in the
415 model could explain the OOA underprediction in Paris. Furthermore, Fountoukis et al.
416 (2014b) evaluated PMCAMx against OOA factor-analysis AMS measurements from several
417 sites all over Europe (Fountoukis et al., 2014b) during a wintertime period (February/March
418 2009) and an autumn period (September/October 2008) and showed good agreement with
419 observations from both periods (mean bias = 0.4 μg m^{-3} and -0.2 μg m^{-3} respectively).
420 Contrary to the present study though, the measurement sites in Fountoukis et al. (2014b)
421 study included only rural and remote areas, while the more than 3 μg m^{-3} of OOA observed in
422 Paris is a lot higher than other wintertime measurements in Europe.

Other possible sources of uncertainty that are not explored here but have been investigated in past applications of PMCAMx include uncertainties in the aging scheme, the magnitude of IVOC emissions, aqueous secondary OA formation and others (Murphy et al., 2011, 2012; Tsimpidi et al., 2010). These studies have shown so far that the base-case OA scheme used in PMCAMx represents reasonably well the average atmospheric chemistry of OA.

5.4 Black Carbon

More than 70% of the hourly summertime BC data are predicted within a factor of two from all three sites (Fig. 5). The model, in agreement with the measurements, predicts the largest BC concentrations in the city center and the lowest at the suburban site of SIRTA. The overall mean bias (0.05 μg m^{-3}) shows encouraging agreement without any systematic errors. During the winter period, with the exception of SIRTA where only 12-hour data were available, the model performs similarly to the summer period with 68% of the data predicted within a factor of two (Fig. 5). A slightly higher overprediction is seen in LHVP (mean bias = 0.5 μg m^{-3}) compared to the summer period (Fig. S1). Both the model and the observations show higher BC concentrations in GOLF than in the city center due to a strong influence of nearby traffic.

Figure 6 shows the average diurnal profile of predicted and observed BC concentrations. PMCAMx does a reasonable job in predicting the low concentrations (minima of the curves) of BC during both periods and in both the city center and the suburbs reproducing even the low levels of BC in SIRTA (down to 0.3 μg m^{-3} in the evening). The small overpredictions in LHVP during summer and in both LHVP and GOLF during winter are mostly during the morning peak and could be related to errors in the traffic emission

447 inventory, errors in the geographical distribution of emissions in the high resolution inventory
448 (Fountoukis et al., 2013) or to an underestimation of the mixing height by the model.
449 Boundary layer height observations were only available in the SIRTA site.

450 A timeseries analysis of BC concentrations at SIRTA showed that the model
451 overpredicted the morning peak BC concentrations by more than a factor of two on July 13,
452 21 and 29. On July 13 the model-simulated mixing height is within 10% of the observed
453 values while on the other two days the model underestimated the mixing height (up to 1200
454 m for an observed mixing height of about 3000 m during the day). It is difficult to quantify
455 the extent of the error this model underestimation would induce to BC concentrations since
456 the mixing height observations are also uncertain. Hodzic et al. (2009) reported a positive
457 bias of 300–1000 m in the mixing height diagnosed from LIDAR observations (used here), as
458 compared to the one from radiosonde profiles. We corrected the BC concentrations in the
459 Paris city center for the estimated 20% average underprediction of the mixing height during
460 the summer. This slightly improved model performance (MB was reduced from 0.3 μg m^{-3} to
461 -0.1 μg m^{-3}) showing that the mixing height underestimation could partly explain the BC
462 discrepancy. However this is a rather crude correction since a large part (40%) of the city's
463 BC is transported from outside the city (Skyllakou et al., 2014). The model underpredicts the
464 morning rise of the boundary layer during both summer and winter so this could also explain
465 part of the BC underprediction in the morning (Fig. S7). Overall, the model predicts, in
466 agreement with the measurements, surprisingly low concentrations of BC for a megacity of
467 10.5 million inhabitants (Beekmann et al., 2015).
468
469
470

5.5 Estimation of cooking OA emissions

Based on the comparison with the factor-analysis AMS data for COA (Section 5.2) a sensitivity simulation was run in which emissions of primary OA were increased by a factor of 3 during summer and 1.5 during winter to roughly account for the missing cooking emissions. These emissions were geographically distributed in the Paris greater area following the pattern of the population density. It should be noted that since IVOC emissions are assumed to be proportional to the emitted primary OA mass, the addition of COA was accompanied by an increase of the IVOC emissions. The total OC emissions added were 5.3 tons d^{-1} for the summer and 5.1 tons d^{-1} for the winter period, or approximately 80 mg d^{-1} per capita during each period. A distinct diurnal emission profile was used taking into consideration that COA concentrations were characterized by a prominent diurnal pattern with peak values during meal times (Crippa et al., 2013b). A variation of day-to-day emissions was also considered with approximately 18.5% of total weekly COA emitted (per day) on weekend days and 12.5% on weekdays. Figure S8 shows the temporal profile of the added cooking emissions during the summer period. The wintertime temporal profile used slightly differs from the summertime one, since these are based on the observed diurnal patterns of COA concentrations. As expected, PMCAMx predictions for total POA concentrations are much closer to observations when COA emissions are included in the inventory (Fig. 7, Table 4). The average summertime predicted total POA is increased to 0.7 μg m^{-3} and the fractional bias drops from -0.7 to 0.05 while the number of data predicted within a factor of two increases from 30% to 60%. In the other two sites the addition of COA considerably improves model predictions although a systematic underprediction still exists (MB = -0.2 μg m^{-3} in SIRTA and -1 μg m^{-3} in GOLF) which could be due to the simplified approach of distributing the COA emissions by population density in the greater area of Paris.

During the winter period the addition of COA results in a reduced model bias for total POA concentrations in Paris city center (FBIAS drops from -0.3 to -0.01). The model performance for OOA remains practically unchanged with the addition of COA during both seasons (Table 4). Figure 8 shows the averaged diurnal profile of COA concentrations predicted and observed during both seasons in LHVP and SIRTA. In SIRTA the model predicts low concentrations (< 0.5 μg m^{-3}) throughout the day during both seasons in agreement with observations. In the city center the two peaks observed during meal times are reproduced with reasonable accuracy. Interestingly, this agreement is achieved when 50% of the daily cooking emissions are emitted during lunch time (12:00 – 14:00 LT) and only 20% during dinner time (20:00-22:00 LT), although the nighttime maximum COA concentration is higher than the midday maximum (by a factor of two in summer). This is due to a strong vertical mixing during the summer days. During the winter period the addition of cooking OA emissions in the city center decreases the fractional bias for total POA concentrations in LHVP from -0.3 to -0.01 and in general significantly improves model predictions.

In a sensitivity test, we added cooking OA emissions in the entire domain assuming the same emission rate per person as in Paris. This is clearly a crude zeroth order approximation. Addition of cooking OA emissions to the inventory, leads to an increase of the total OA emissions by as much as a factor of 2-3 in some highly populated areas (Fig. S9). These additional European cooking OA emissions do affect OA levels in Paris. Assuming similar chemical aging parameters as for the transportation OA we estimated that these emissions could increase average OA in Paris by 0.1-0.2 μg m^{-3} on average; a small but non-negligible contribution.

519 **6. Conclusions**

520 PMCAMx, a 3-D chemical transport model, was applied using both regional and
521 urban domains to simulate the formation of carbonaceous aerosol during the MEGAPOLI
522 summer and winter campaigns. A high grid resolution over the Paris greater area along with
523 high resolution emissions (4×4 km^2) was used to examine the role of sources and production
524 mechanisms in the organic aerosol and BC concentrations.

525 PMCAMx predicts BC concentrations reasonably well during both periods and in
526 both the city center and the suburbs (FBIAS = -0.1 in summer and 0.1 in winter) reproducing
527 the majority (70%) of the hourly data within a factor of two. The largest source of
528 summertime BC concentrations is traffic (70%) and of wintertime the residential combustion
529 (45%). Almost 60% of the BC is predicted to originate from local sources during both
530 summer and winter.

531 The agreement for the summertime secondary OA concentrations is also encouraging
532 (mean bias = 0.1 μg m^{-3}) highlighting the ability of the model to reproduce the major
533 secondary OA transport and transformation processes during a photochemically intense
534 period. The model predicts that during the summer a large fraction (54%) of the OOA
535 concentration in the city center is comprised of SOA from biogenic VOCs followed by SOA
536 from semi-volatile and intermediate-volatility VOCs (33%) while a smaller fraction (13%)
537 consists of SOA from anthropogenic VOCs.

538 Wintertime simulations showed a surprisingly large underestimation of OOA in the
539 Paris greater area (mean bias = -2.3 μg m^{-3}) that has not been reported in any of the previous
540 applications of the model in either the European or the United States domain. A process
541 forming secondary OA (in a polluted environment with high NO_x concentrations and in the
542 absence of light) that is not simulated in the model could partly explain this underprediction.

543 The model evaluation for primary OA concentrations revealed a major deficiency of
544 the emission inventory, namely the missing primary organic aerosol emissions from cooking
545 activities during both summer and winter. Based on the comparison with the factor-analysis
546 AMS data for cooking OA, more than 5 tons d^{-1} (or 80 mg d^{-1} per capita) should be added in
547 the emission inventory with a distinct diurnal profile in which 50% of the daily cooking
548 emissions are emitted during lunch time (12:00 – 2:00 pm) and 20% during the dinner time
549 (8:00-10:00 pm). This addition improved significantly the model performance for both
550 summer and winter. This work strongly supports that much more attention should be paid to
551 the OA emission inventories of megacities and more specifically to the cooking source sector.
552 However, the remarkable diurnal variation of these emissions shows that more research is
553 also needed towards a better understanding of which activities contribute to these emissions
554 (e.g. meat grilling is one known important source of COA).
555 Focusing on ambient primary OA concentrations, the cooking source seems to be an
556 attractive target for pollution reduction strategies since COA contributes 70% to total primary
557 OA concentrations during summer. During winter both cooking (40%) and biomass burning
558 (40%) are the two major contributors. Focusing on reducing BC concentrations, however, the
559 traffic sector deserves the most attention during summer with the addition of residential
560 combustion in winter.
561
562 **Acknowledgements**
563 This work was funded by the EU FP7 project MEGAPOLI (Grant Agreement no.: 212520),
564 the EU FP7 IDEAS ATMOPACS project (grant agreement 267099) and the ARISTEIA
565 ROMANDE project (National Research Excellence Grant).

References

Airparif, 2010. Ile-de-France gridded emission inventory 2005 (version 2008), http://www.airparif.asso.fr/.

Allan, J. D., Williams, P. I., Morgan, W. T., Martin, C. L., Flynn, M. J., Lee, J., Nemitz, E., Phillips, G. J., Gallagher, M. W., and Coe, H.: Contributions from transport, solid fuel burning and cooking to primary organic aerosols in two UK cities, Atmos. Chem. and Phys., 10, 647-668, 2010.

Atkinson, R., Arey, J.: Atmospheric degradation of volatile organic compounds. Chemical Reviews, 103, 4605 - 4638, 2003.

Beekmann, M., Prevot, A. S. H., Drewnick, F., Sciare, J., Pandis, S. N., Denier van der Gon, H. A. C., Crippa, M., Freutel, F., Poulain, L., Ghersi, V., Rodriguez, E., Beirle, S., Zotter, P., von der Weiden-Reinmüller, S.-L., Bressi, M., Fountoukis, C., Petetin, H., Szidat, S., Schneider, J., Rosso, A., El Haddad, I., Megaritis, A., Zhang, Q. J., Slowik, J. G., Moukhtar, S., Kolmonen, P., Stohl, A., Eckhardt, S., Borbon, A., Gros, V., Marchand, N., Jaffrezo, J. L., Schwarzenboeck, A., Colomb, A., Wiedensohler, A., Borrmann, S., Lawrence, M., Baklanov, A., and Baltensperger, U.: In-situ, satellite measurement and model evidence for a dominant regional contribution to fine particulate matter levels in the Paris Megacity, Atmos. Chem. Phys. Discuss., 15, 8647–8686, 2015.

Bergstrom, R., Denier van der Gon, H. A. C., Prevot, A. S. H., Yttri, K. E., Simpson, D.: Modelling of organic aerosols over Europe (2002-2007) using a volatility basis set (VBS) framework: application of different assumptions regarding the formation of secondary organic aerosol. Atmos. Chem. Phys. 12, 8499 - 8527, http://dx.doi.org/10.5194/acp-12-8499 - 2012, 2012.

Bougiatioti, A., Stavroulas, I., Kostenidou, E., Zarmpas, P., Theodosi, C., Kouvarakis, G., Canonaco, F., Prévôt, A. S. H., Nenes, A., Pandis, S. N., and Mihalopoulos, N.: Processing of biomass-burning aerosol in the eastern Mediterranean during summertime, Atmos. Chem. Phys., 14, 4793 - 4807, 2014.

Canonaco, F., Crippa, M., Slowik, J. G., Baltensperger, U., and Prévôt, A. S. H.: SoFi, an Igor based interface for the efficient use of the generalized multilinear engine (ME-2) for

595 source apportionment: application to aerosol mass spectrometer data, Atmos. Meas. Tech.,
596 6, 3649–3661, 2013.

597 Couvidat, F., Kim, Y., Sartelet, K., Seigneur, C., Marchand, N., and Sciare, J.: Modeling
598 secondary organic aerosol in an urban area: application to Paris, France, Atmos. Chem.
599 Phys., 13, 983–996, doi:10.5194/acp-13-983-2013, 2013.

600 Crippa, M., DeCarlo, P. F., Slowik, J. G., Mohr, C., Heringa, M. F., Chirico, R., Poulain, L.,
601 Freutel, F., Sciare, J., Cozic, J., Di Marco, C. F., Elsasser, M., Nicolas, J. B., Marchand,
602 N., Abidi, E., Wiedensohler, A., Drewnick, F., Schneider, J., Borrmann, S., Nemitz, E.,
603 Zimmermann, R., Jaffrezo, J. L., Prévôt, A. S. H., and Baltensperger, U.: Wintertime
604 aerosol chemical composition and source apportionment of the organic fraction in the
605 metropolitan area of Paris, Atmos. Chem. Phys., 13, 961 - 981, doi:10.5194/acp-13-961-
606 2013, 2013a.

607 Crippa, M., F. Canonaco, J. G. Slowik, I. El Haddad, P. F. DeCarlo, C. Mohr, M. F. Heringa,
608 R. Chirico, N. Marchand, B. Temime-Roussel, E. Abidi, L. Poulain, A. Wiedensohler, U.
609 Baltensperger, and A. S. H. Prevot, Primary and secondary organic aerosol origin by
610 combined gas-particle phase source apportionment, Atmos. Chem. Phys., 13, 8411 - 8426,
611 2013b.

612 Crippa, M., El Haddad, I., Slowik, J. G., DeCarlo, P. F., Mohr, C., Heringa, M. F., Chirico,
613 R., Marchand, N., Sciare, J., Baltensperger, U., and Prévôt, A. S. H.: Identification of
614 marine and continental aerosol sources in Paris using high resolution aerosol mass
615 spectrometry, J. Geophys. Res., 118, 1950 - 1963, doi:10.1002/jgrd.50151, 2013c.

616 DeCarlo, P. F., Kimmel, J. R., Trimborn, A., Northway, M. J., Jayne, J. T., Aiken, A. C.,
617 Gonin, M., Fuhrer, K., Horvath, T., Docherty, K. S., Worsnop, D. R., and Jimenez, J. L.:
618 Field-deployable, high-resolution, time-of-flight aerosol mass spectrometer, Anal. Chem.,
619 78, 8281 - 8289, 2006.

620 Denier van der Gon, H.A.C., Beevers, S., D'Allura, Al., Finardi, S., Honoré, C., Kuenen, J.,
621 Perrussel, O., Radice, P., Theloke, J., Uzbasich, M., Visschedijk, A., 2011. Discrepancies
622 Between Top-Down and Bottom-Up Emission Inventories of Megacities: The Causes and
623 Relevance for Modeling Concentrations and Exposure In: D.G. Steyn and S.T. Castelli

(eds.), NATO Science for Peace and Security Series C: Environmental Security, Vol. 4, Springer, ISBN 978-94-007-1358-1, p. 772.

Denier van der Gon, H. A. C., Bergström, R., Fountoukis, C., Johansson, C., Pandis, S. N., Simpson, D., and Visschedijk, A.: Particulate emissions from residential wood combustion in Europe – revised estimates and an evaluation, Atmos. Chem. Phys. Discuss., 14, 31719-31765, 2014.

Donahue, N.M., Robinson, A.L., Stanier, C.O., Pandis, S.N., 2006. Coupled partitioning, dilution, and chemical aging of semivolatile organics, Environmental Science and Technology, 40, 2635 - 2643.

Donahue, N. M., Robinson, A.L., Pandis, S.N., 2009. Atmospheric organic particulate matter: From smoke to secondary organic aerosol. Atmospheric Environment, 43, 94 - 106.

Drewnick, F., Hings, S. S., DeCarlo, P., Jayne, J. T., Gonin, M., Fuhrer, K., Weimer, S., Jimenez, J. L., Demerjian, K. L., Borrmann, S., and Worsnop, D. R.: A new time-of-flight aerosol mass spectrometer (TOF-AMS) – Instrument description and first field deployment, Aerosol Sci. Technol., 39, 637–658, 2005.

ENVIRON, User's Guide to the Comprehensive Air Quality Model with Extensions (CAMx), Version 4.02, Report, ENVIRON Int. Corp., Novato, Calif, available at: http://www.camx.com, 2003.

Fast, J., Aiken, A. C., Allan, J., Alexander, L., Campos, T., Canagaratna, M. R., Chapman, E., DeCarlo, P. F., de Foy, B., Gaffney, J., de Gouw, J., Doran, J. C., Emmons, L., Hodzic, A., Herndon, S. C., Huey, G., Jayne, J. T., Jimenez, J. L., Kleinman, L., Kuster, W., Marley, N., Russell, L., Ochoa, C., Onasch, T. B., Pekour, M., Song, C., Ulbrich, I. M., Warneke, C., Welsh- Bon, D., Wiedinmyer, C., Worsnop, D. R., Yu, X. Y., and Zaveri, R.: Evaluating simulated primary anthropogenic and biomass burning organic aerosols during MILAGRO: implications for assessing treatments of secondary organic aerosols, Atmos. Chem. Phys., 9, 6191–6215, doi:10.5194/acp-9-6191-2009, 2009.

Favez, O., Cachier, H., Sciare, J., Le Moullec, Y.: Characterization and contribution to $PM_{2.5}$ of semi-volatile aerosols in Paris (France), Atmos. Environ. 41, 7969 - 7976, 2007.

Fountoukis, C., Racherla, P. N., Denier van der Gon, H. A. C., Polymeneas, P., Haralabidis, P. E., Wiedensohler, A., Pilinis, C., and Pandis, S. N: Evaluation of a three-dimensional

654 chemical transport model (PMCAMx) in the European domain during the EUCAARI May
655 2008 campaign, Chem. Phys., 11, 14183 - 14220, 2011.

656 Fountoukis, C., Koraj, D., Denier van der Gon, H. A. C., Charalampidis, P. E., Pilinis, C., and
657 Pandis, S. N.: Impact of grid resolution on the predicted fine PM by a regional 3-D
658 chemical transport model, Atmos. Environ., 68, 24 - 32, 2013.

659 Fountoukis, C., T. Butler, M. G. Lawrence, H. A. C. Denier van der Gon, A. J. H.
660 Visschedijk, P. Charalampidis, C. Pilinis, and S. N. Pandis: Impacts of controlling biomass
661 burning emissions on wintertime carbonaceous aerosol in Europe, Atmos. Environ. 87,
662 175 - 182, 2014a.

663 Fountoukis, C., Megaritis, A. G., Skyllakou, K., Charalampidis, P. E., Pilinis, C., Denier van
664 der Gon, H. A. C., Crippa, M., Canonaco, F., Mohr., C., Prévôt, A. S. H., Allan, J. D.,
665 Poulain, L., Petäjä, T., Tiitta, P., Carbone, S., Kiendler-Scharr, A., Nemitz, E., O'Dowd,
666 C., Swietlicki, E., and Pandis, S.N.: Organic aerosol concentration and composition over
667 Europe: Insights from comparison of regional model predictions with aerosol mass
668 spectrometer factor analysis, Atmos. Chem. Phys., 14, 9061 - 9076, 2014b.

669 Freney, E.J., K. Sellegri, F. Canonaco, A. Colomb, A. Borbon, V. Michoud, J.-F. Doussin, S.
670 Crumeyrolle, N. Amarouch, J.-M. Pichon, A. S. H. Prévôt, M. Beekmann, and A.
671 Schwarzenböeck, Characterizing the impact of urban emissions on regional aerosol
672 particles; airborne measurements during the MEGAPOLI experiment, Atmos. Chem.
673 Phys. Discuss., 13, 24885 - 24924, 2013.

674 Freutel, F., Schneider, J., Drewnick, F., von der Weiden-Reinmüller, S.-L., Crippa, M.,
675 Prévôt, A. S. H., Baltensperger, U., Poulain, L., Wiedensohler, A., Sciare, J., Sarda-
676 Estève, R., Burkhart, J. F., Eckhardt, S., Stohl, A., Gros, V., Colomb, A., Michoud, V.,
677 Doussin, J. F., Borbon, A., Haeffelin, M., Morille, Y., Beekmann, M., and Borrmann, S.:
678 Aerosol particle measurements at three stationary sites in the megacity of Paris during
679 summer 2009: meteorology and air mass origin dominate aerosol particle composition and
680 size distribution, Atmos. Chem. Phys., 13, 933 - 959, doi:10.5194/acp-13-933-2013, 2013.

681 Guenther, A., Karl, T., Harley, P., Wiedinmyer, C., Palmer, P. I., Geron, C.: Estimates of
682 global terrestrial isoprene emissions using MEGAN (Model of Emissions of Gases and

683 Aerosols from Nature). Atmos. Chem. Phys. 6, 3181 - 3210, doi:10.5194/acp-6-3181-
684 2006, 2006.

685 Haeffelin, M., Barthès, L., Bock, O., Boitel, C., Bony, S., Bouniol, D., Chepfer, H., Chiriaco,
686 M., Cuesta, J., Delanoë, J., Drobinski, P., Dufresne, J.-L., Flamant, C., Grall, M., Hodzic,
687 A., Hourdin, F., Lapouge, F., Lemaitre, Y., Mathieu, A., Morille, Y., Naud, C., Noel, V.,
688 O'Hirok, W., Pelon, J., Pietras, C., Protat, A., Romand, B., Scialom, G., and Vautard, R.:
689 SIRTA, a ground-based atmospheric observatory for cloud and aerosol research, Ann.
690 Geophys., 23, 253 - 275, doi:10.5194/angeo-23-253-2005, 2005.

691 Hallquist, M., Wenger, J. C., Baltensperger, U., Rudich, Y., Simpson, D., Claeys, M.,
692 Dommen, J., Donahue, N. M., George, C., Goldstein, A. H., Hamilton, J. F., Herrmann,
693 H., Hoffmann, T., Iinuma, Y., Jang, M., Jenkin, M. E., Jimenez, J. L., Kiendler-Scharr, A.,
694 Maenhaut, W., McFiggans, G., Mentel, Th. F., Monod, A., Prevot, A. S. H., Seinfeld, J.
695 H., Surratt, J. D., Szmigielski, R., and Wildt, J.: The formation, properties and impact of
696 secondary organic aerosol: current and emerging issues, Atmos. Chem. Phys., 9, 5155 -
697 5236, 2009.

698 Healy, R. M., Sciare, J., Poulain, L., Kamili, K., Merkel, M., Muller, T., Wiedensohler, A.,
699 Eckhardt, S., Stohl, A., Sarda-Esteve, R., McGillicuddy, E., O'Connor, I. P., Sodeau, J. R.,
700 and Wenger, J. C.: Sources and mixing state of size-resolved elemental carbon particles in
701 a European megacity: Paris, Atmos. Chem. Phys., 12, 1681 - 1700, doi:10.5194/acp-12-
702 1681-2012, 2012.

703 Hersey, S. P., Craven, J. S., Schilling, K. A., Metcalf, A. R., Sorooshian, A., Chan, M. N.,
704 Flagan, R. C., and Seinfeld, J. H.: The Pasadena Aerosol Characterization Observatory
705 (PACO): chemical and physical analysis of the Western Los Angeles basin aerosol,
706 Atmos. Chem. Phys., 11, 7417 - 7443, doi:10.5194/acp-11-7417-2011, 2011.

707 Hodzic, A., Jimenez, J. L., Madronich, S., Aiken, A. C., Bessagnet, B., Curci, G., Fast, J.,
708 Lamarque, J.-F., Onasch, T. B., Roux,G., Schauer, J. J., Stone, E. A., and Ulbrich, I. M.:
709 Modeling organic aerosols during MILAGRO: importance of biogenic secondary organic
710 aerosols, Atmos. Chem. Phys., 9, 6949 - 6981, doi:10.5194/acp-9-6949-2009, 2009.

711 Kostenidou, E., Kaltsonoudis, C., Tsiflikiotou, M., Louvaris, E., Russell, L. M., Pandis, S. N.:
712 Burning of olive tree branches: a major organic aerosol source in the Mediterranean,
713 Atmos. Chem. Phys., 13, 8797 - 8811, 2013.

714 Kuenen, J., Denier van der Gon, H., Visschedijk, A., van der Brugh, H., Finardi, S., Radice,
715 P., d'Allura, A., Beevers, S., Theloke, J., Uzbasich, M., Honoré, C., Perrussel, O., 2010.
716 MEGAPOLI Scientific Report 10-17: A Base Year (2005) MEGAPOLI European Gridded
717 Emission Inventory. MEGAPOLI Deliverable D1.6.

718 Lane, T.E., Donahue, N.M., Pandis, S.N.: Simulating secondary organic aerosol formation
719 using the volatility basis-set approach in a chemical transport model, Atmospheric
720 Environment, 42, 7439 - 7451, 2008.

721 Molina, L. T., Madronich, S., Gaffney, J. S., Apel, E., de Foy, B., Fast, J., Ferrare, R.,
722 Herndon, S., Jimenez, J. L., Lamb, B., Osornio-Vargas, A. R., Russell, P., Schauer, J. J.,
723 Stevens, P. S., Volkamer, R., and Zavala, M.: An overview of the MILAGRO 2006
724 Campaign: Mexico City emissions and their transport and transformation, Atmos. Chem.
725 Phys., 10, 8697–8760, doi:10.5194/acp-10-8697-2010, 2010.

726 O'Dowd, C.D., Langmann, B., Varghese, S., Scannell, C., Ceburnis, D., Facchini, M.C.: A
727 combined organic-inorganic sea-spray source function. Geophysical Research Letters 35,
728 L01801, doi:10.1029/2007GL030331, 2008.

729 Paatero, P.: The multilinear engine - A table-driven, least squares program for solving
730 multilinear problems, including the n-way parallel factor analysis model, J. Comput.
731 Graph. Stat., 8, 854-888, 1999.

732 Pouliot, G., Pierce, T, Denier van der Gon, H., Schaap, M., Nopmongcol, U.: Comparing
733 Emissions Inventories and Model-Ready Emissions Datasets between Europe and North
734 America for the AQMEII Project. Atmos. Environ. (AQMEII issue) 53, 4 – 14, 2012.

735 Robinson, A. L., Donahue, N. M., Shrivastava, M. K., Weitkamp, E. A., Sage, A. M.,
736 Grieshop, A. P., Lane, T. E., Pierce, J. R., and Pandis, S. N.: Rethinking organic aerosols:
737 Semi-volatile emissions and photochemical aging, Science, 315, 1259–1262, 2007.

738 Sciare, J., d'Argouges, O., Zhang, Q. J., Sarda-Estève, R., Gaimoz, C., Gros, V., Beekmann,
739 M., and Sanchez, O.: Comparison between simulated and observed chemical composition
740 of fine aerosols in Paris (France) during springtime: contribution of regional versus

741 continental emissions, Atmos. Chem. Phys., 10, 11987 - 12004, doi:10.5194/acp-10-
742 11987-2010, 2010.

743 Seinfeld, J. H. and Pandis, S. N.: Atmospheric chemistry and physics: From air pollution to
744 climate change. 2nd ed.; John Wiley and Sons, Hoboken, NJ, 2006.

745 Shrivastava, M.K., Lane, T.E., Donahue, N.M., Pandis, S.N., and Robinson, A.L., 2008.
746 Effects of gas-particle partitioning and aging of primary emissions on urban and regional
747 organic aerosol concentrations, Journal of Geophysical Research, 113, D18301,
748 doi:10.1029/2007JD009735.

749 Skamarock, W.C., Klemp, J.B., Dudhia, J., Gill, D.O., Barker, D.M., Wang, W., Powers,
750 J.G., 2005. A Description of the Advanced Research WRF Version 2. NCAR Technical
751 Note (http://www.mmm.ucar.edu/wrf/users/docs/arwv2.pdf).

752 Skyllakou, K., Murphy, B. N., Megaritis, A. G., Fountoukis, C., and Pandis, S. N.:
753 Contributions of local and regional sources to fine PM in the Megacity of Paris, Atmos.
754 Chem. Phys., 14, 2343 - 2352, 2014.

755 Sofiev, M., Vankevich, R., Lotjonen, M., Prank, M., Petukhov, V., Ermakova, T., Koskinen,
756 J., Kukkonen, J.: An operational system for the assimilation of the satellite information on
757 wild-land fires for the needs of air quality modeling and forecasting, Atmos. Chem. Phys.
758 9, 6833 - 6847, 2009.

759 Sun, J., Zhang, Q., Canagaratna, M. R., Zhang, Y., Ng, N. L., Sun, Y., Jayne, J. T., Zhang,
760 X., Zhang, X., and Worsnop, D. R.: Highly time- and size-resolved characterization of
761 submicron aerosol particles in Beijing using an Aerodyne Aerosol Mass Spectrometer,
762 Atmos. Environ., 44, 131 - 140, doi:10.1016/j.atmosenv.2009.03.020, 2010.

763 Sun, Y.-L., Zhang, Q., Schwab, J. J., Demerjian, K. L., Chen, W.-N., Bae, M.-S., Hung, H.-
764 M., Hogrefe, O., Frank, B., Rattigan, O. V., and Lin, Y.-C.: Characterization of the
765 sources and processes of organic and inorganic aerosols in New York city with a high-
766 resolution time-of-flight aerosol mass spectrometer, Atmos. Chem. Phys., 11, 1581–1602,
767 doi:10.5194/acp-11-1581-2011, 2011.

768 Tsimpidi, A.P., Karydis, V.A., Zavala, M., Lei, W., Molina, L., Ulbrich, I.M., Jimenez, J.L.,
769 Pandis, S.N.: Evaluation of the volatility basis-set approach for the simulation of organic

770 aerosol formation in the Mexico City metropolitan area, Atmos. Chem. Phys., 10, 525 –
771 546, 2010.

772 Ulbrich, I. M., Canagaratna, M. R., Zhang, Q., Worsnop, D. R., and Jimenez, J. L.:
773 Interpretation of organic components from positive matrix factorization of aerosol mass
774 spectrometric data, Atmos. Chem. Phys., 9, 2891-2918, 2009.

775 Visschedijk, A. J. H., Zandveld, P., and Denier van der Gon, H. A. C.: TNO Report 2007 A-
776 R0233/B: A high resolution gridded European emission database for the EU integrated
777 project GEMS, Netherlands, Organization for Applied Scientific Research, 2007.

778 Xing, J.-H., Takahashi, K., Yabushita, A., Kinugawa, T., Nakayama, T., Matsumi, Y.,
779 Tonokura, K., Takami, A., Imamura, T., Sato, K., Kawasaki, M., Hikida, T., and Shimono,
780 A.: Characterization of Aerosol Particles in the Tokyo Metropolitan Area using Two
781 Different Particle Mass Spectrometers, Aerosol Sci. Technol., 45, 315–326, 2011.

782 Zhang, Q., Jimenez, J. L., Canagaratna, M. R., Allan, J. D., Coe, H., Ulbrich, I., Alfarra, M.
783 R., Takami, A., Middlebrook, A. M., Sun, Y. L., Dzepina, K., Dunlea, E., Docherty, K.,
784 De-Carlo, P., Salcedo, D., Onasch, T. B., Jayne, J. T., Miyoshi, T., Shimono, A.,
785 Hatakeyama, N., Takegawa, N., Kondo, Y., Schneider, J., Drewnick, F., Weimer, S.,
786 Demerjian, K. L., Williams, P. I., Bower, K. N., Bahreini, R., Cottrell, L., Griffin, R. J.,
787 Rautianen, J., and Worsnop, D. R.: Ubiquity and dominance of oxygenated species in
788 organic aerosols in anthropogenicallyinfluenced Northern Hemisphere midlatitudes,
789 Geophys. Res. Lett., 34, L13801, doi:10.1029/2007GL029979, 2007.

790 Zhang, Q. J., Beekmann, M., Drewnick, F., Freutel, F., Schneider, J., Crippa, M., Prévôt, A.
791 S. H., Baltensperger, U., Poulain, L., Wiedensohler, A., Sciare, J., Gros, V., Borbon, A.,
792 Colomb, A., Michoud, V., Doussin, J.-F., Denier van der Gon, H. A. C., Haeffelin, M.,
793 Dupont, J.-C., Siour, G., Petetin, H., Bessagnet, B., Pandis, S. N., Hodzic, A., Sanchez, O.,
794 Honoré, C., and Perrussel, O.: Formation of organic aerosol in the Paris region during the
795 MEGAPOLI summer campaign: evaluation of the volatility-basis-set approach within the
796 CHIMERE model, Atmos. Chem. Phys., 13, 5767–5790, doi:10.5194/acp-13-5767-2013,
797 2013.

798

799 **Table 1**. Emission mass totals (in tons/month) for the Paris greater area as shown in Fig. 1.

Species	CO	NO	SO_2	NH_3	VOCs			Nitrate	Sulfate	Ammonium	BC	OC	Sodium	Chloride
					Isoprene	MT[1]	Other[2]							
							Summer 2009							
Anthropogenic	27307	10562	556	1877	-	-	12042	-	44	-	455	1058	12	-
Natural (land)	2247	204	-	-	2861	1435	2390	-	-	-	-	-	-	-
Natural (Fires)	340	10	2	5	-	-	5	3	7	1	7	23	-	-
							Winter 2010							
Anthropogenic	54041	15440	5713	1999	-	-	17089	-	158	-	726	1892	32	-
Natural (land)	314	30	-	-	26	211	301	-	-	-	-	-	-	-

800 [1] MT: Monoterpene emissions

801 [2] Other: Other VOCs excluding methane and methanol

802 **Table 2.** OA components identified by the PMF analysis in each site during the MEGAPOLI summer and winter campaigns

803

OA components	Summer	Winter
LHVP	HOA, COA	HOA, BBOA, COA
	LV-OOA, SV-OOA, MOA	OOA1, OOA2
SIRTA	HOA, COA	HOA, BBOA, COA
	LV-OOA, SV-OOA, MOA	OOA
GOLF	HOA	HOA, BBOA
	OOA	OOA1, OOA2

804 **Table 3.** Prediction skill metrics of PMCAMx against observed hourly data.

	Summer				Winter			
POA	LHVP	SIRTA	GOLF	Average	LHVP	SIRTA	GOLF	Average
Mean predicted (μg m^{-3})	0.3	0.15	0.2	0.2	2.2	1.4	1.7	1.8
Mean observed (μg m^{-3})	0.7	0.5	1.6	1	2.7	2.4	1.3	2.2
FERROR[1]	0.9	1	1.5	1.1	0.7	0.8	0.65	0.7
FBIAS[2]	-0.7	-0.9	-1.5	-1	-0.3	-0.6	0.2	-0.3
MAGE[3] (μg m^{-3})	0.4	0.4	1.4	0.8	1.7	1.5	1.1	1.4
MB[4] (μg m^{-3})	-0.3	-0.4	-1.4	-0.8	-0.5	-1	0.4	-0.4
OOA								
Mean predicted (μg m^{-3})	1.6	1.5	1.6	1.5	0.9	0.8	0.9	0.9
Mean observed (μg m^{-3})	1.7	1.2	1.5	1.4	3.2	3.3	3	3.2
FERROR	0.3	0.4	0.4	0.4	1.1	1.2	1.1	1.1
FBIAS	-0.05	0.2	0.02	0.05	-1.1	-1.1	-1	-1.1
MAGE (μg m^{-3})	0.4	0.5	0.5	0.5	2.3	2.5	2.1	2.3
MB (μg m^{-3})	-0.1	0.3	0.07	0.1	-2.3	-2.5	-2	-2.3
BC								
Mean predicted (μg m^{-3})	1.6	0.6	1	1	1.9	1.8	2.3	2.1
Mean observed (μg m^{-3})	1.3	0.65	1.1	1	1.4	0.9	2.1	1.8
FERROR	0.5	0.6	0.4	0.5	0.5	-	0.5	0.5
FBIAS	0.07	-0.2	-0.1	-0.1	0.2	-	0.02	0.1
MAGE (μg m^{-3})	0.9	0.4	0.5	0.6	1	-	1.2	1.1
MB (μg m^{-3})	0.3	-0.05	-0.05	0.05	0.5	-	0.2	0.3

805 [1] $FERROR = 2/n \sum_{i=1}^{n} |P_i - O_i| / (P_i + O_i)$, where P_i represents the model predicted value for data
806 point i, O_i is the corresponding observed value and n is the total number of data points.

807 [2] $FBIAS = 2/n \sum_{i=1}^{n} (P_i - O_i) / (P_i + O_i)$

808 [3] $MAGE = 1/n \sum_{i=1}^{n} |P_i - O_i|$

809 [4] $MB = 1/n \sum_{i=1}^{n} (P_i - O_i)$

Table 4. Prediction skill metrics of PMCAMx with the addition of COA against observed hourly data.

	Summer				Winter			
POA	LHVP	SIRTA	GOLF	Average	LHVP	SIRTA	GOLF	Average
Mean predicted (μg m^{-3})	0.7	0.3	0.6	0.6	3	1.7	2	2.3
Mean observed (μg m^{-3})	0.7	0.5	1.6	1	2.7	2.4	1.3	2.2
FERROR	0.6	0.8	0.9	0.7	0.6	0.7	0.7	0.7
FBIAS	0.05	-0.5	-0.8	-0.5	-0.01	-0.5	0.3	-0.1
MAGE (μg m^{-3})	0.4	0.3	1	0.6	2	1.5	1.3	1.6
MB (μg m^{-3})	0.05	-0.2	-1	-0.4	0.5	-0.8	0.8	0.1
OOA								
Mean predicted (μg m^{-3})	1.6	1.5	1.6	1.5	0.8	0.7	0.8	0.8
Mean observed (μg m^{-3})	1.7	1.2	1.5	1.4	3.2	3.3	3	3.2
FERROR	0.3	0.4	0.4	0.4	1.1	1.2	1.1	1.1
FBIAS	-0.05	0.1	0.02	0.05	-1.1	-1.1	-1	-1.1
MAGE (μg m^{-3})	0.5	0.5	0.5	0.5	2.3	2.6	2.1	2.3
MB (μg m^{-3})	-0.1	0.3	0.08	0.1	-2.3	-2.6	-2	-2.3

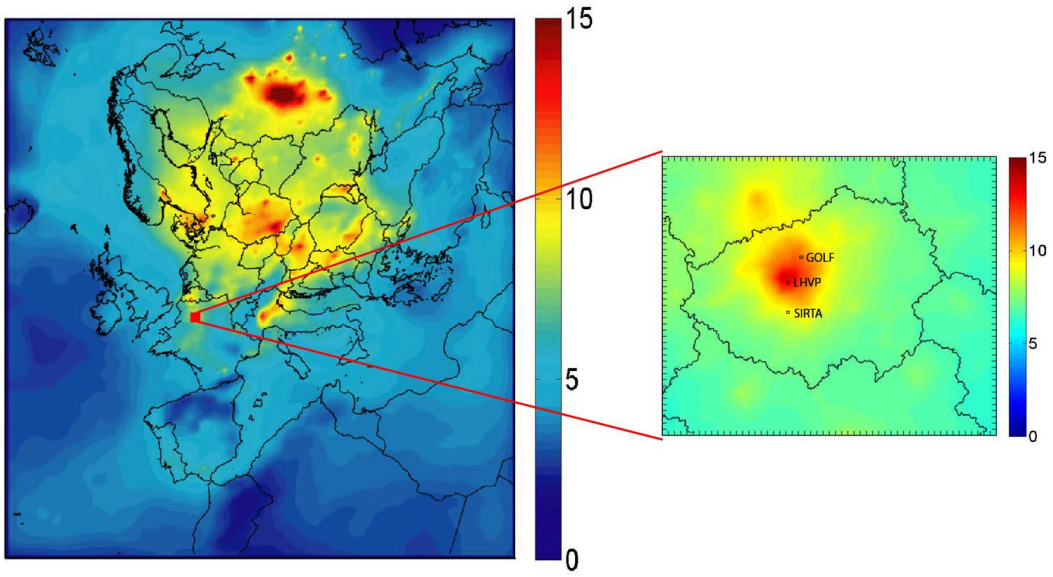

Figure 1. Modeling domain of PMCAMx for Europe. Also shown are the three measurement stations in the nested 4×4 km^2 subdomain of Paris. Color coding shows the predicted average ground concentrations (in $\mu g\ m^{-3}$) of PM_1 during winter 2010.

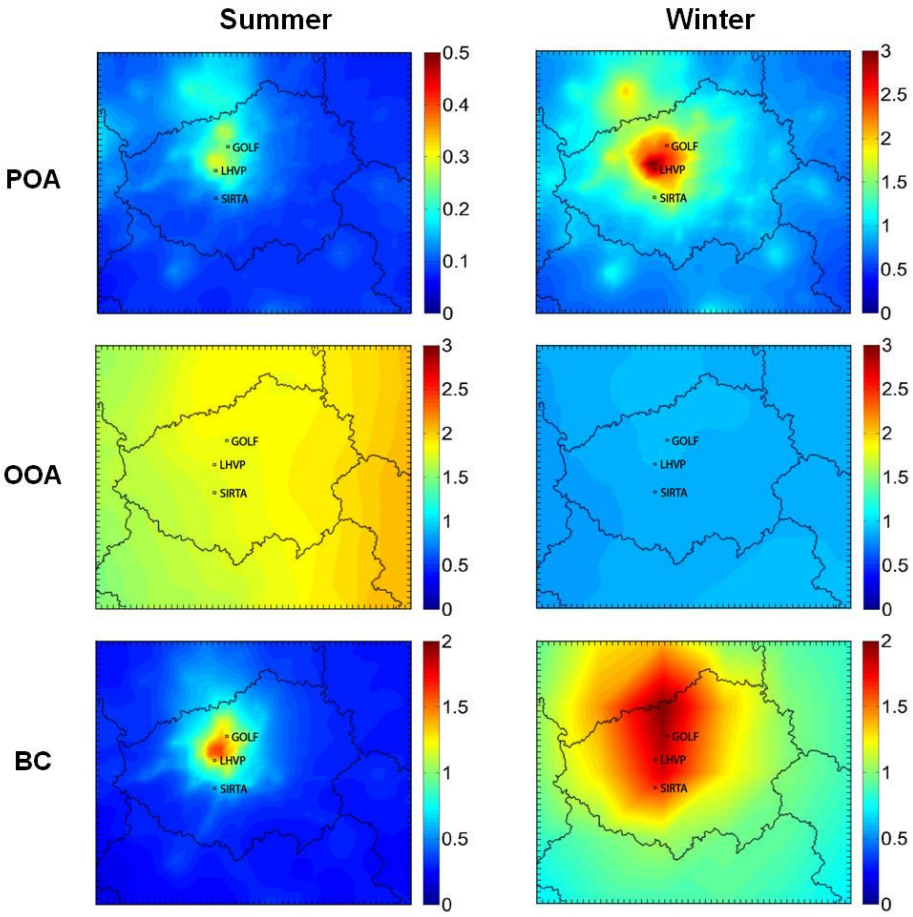

Figure 2. Predicted average ground concentrations (in μg m^{-3}) of fine fresh total POA, BC and OOA in the greater area of Paris during summer 2009 and winter 2010. Different scales are used.

825

826

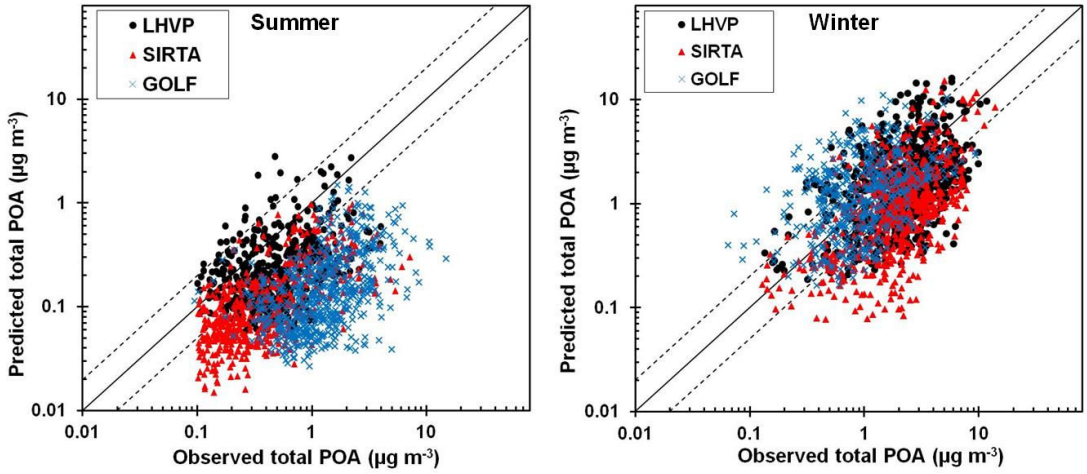

827

828 **Figure 3.** Comparison of predicted vs. observed PM_1 total POA (µg m^{-3}) from the three
829 measurement stations during the MEGAPOLI summer and winter campaigns. Each point is
830 an hourly average value. Also shown are the 1:1, 2:1 and 1:2 lines. Observed data represent
831 AMS factor-analysis results.

832

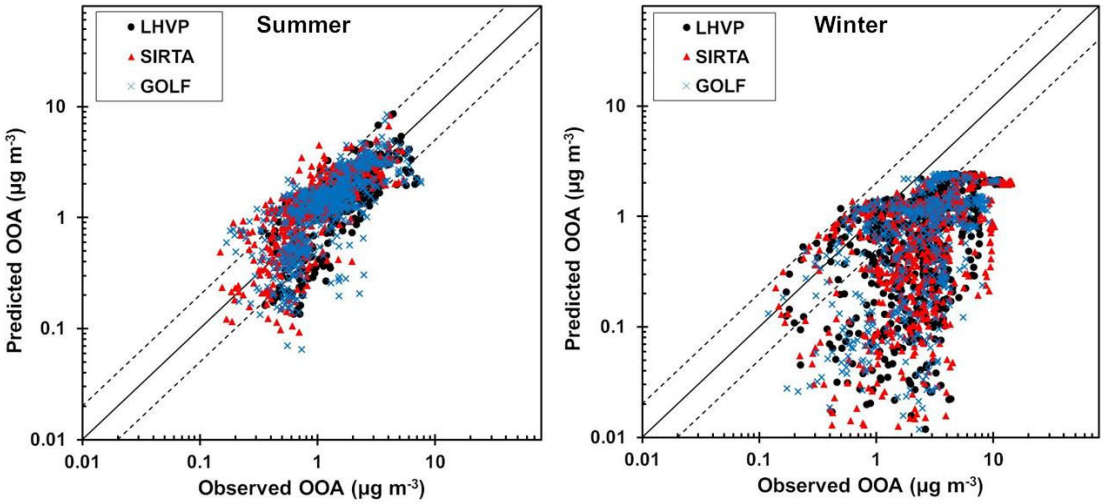

Figure 4. Comparison of predicted vs. observed PM_1 OOA (µg m^{-3}) from the three measurement stations during the MEGAPOLI summer and winter campaigns. Each point is an hourly average value. Also shown are the 1:1, 2:1 and 1:2 lines. Observed data represent AMS factor-analysis results.

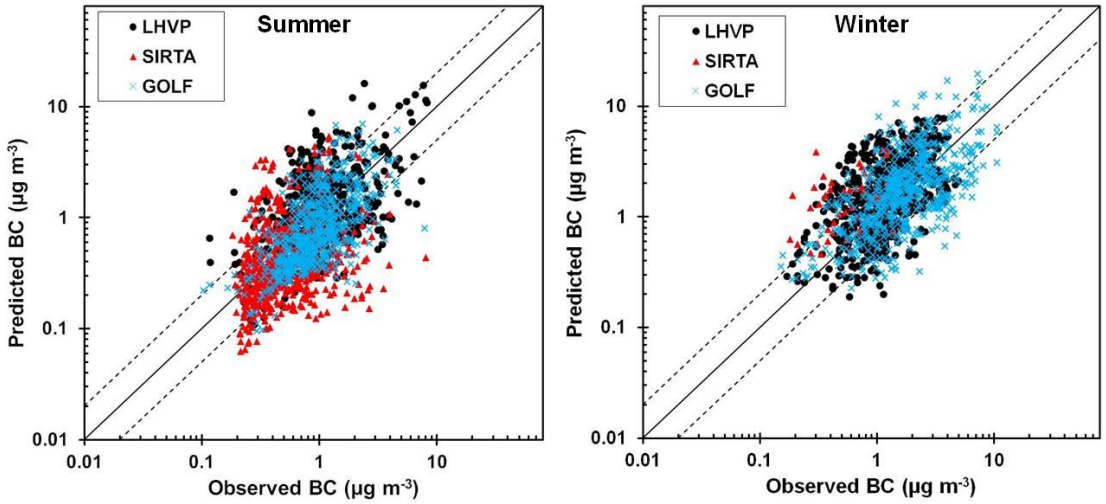

Figure 5. Comparison of predicted vs. observed fine BC (µg m^{-3}) from the three measurement stations during the MEGAPOLI summer and winter campaigns. Each point is an hourly average value with the exception of wintertime data at SIRTA where only 12-hour data were available. Also shown are the 1:1, 2:1 and 1:2 lines.

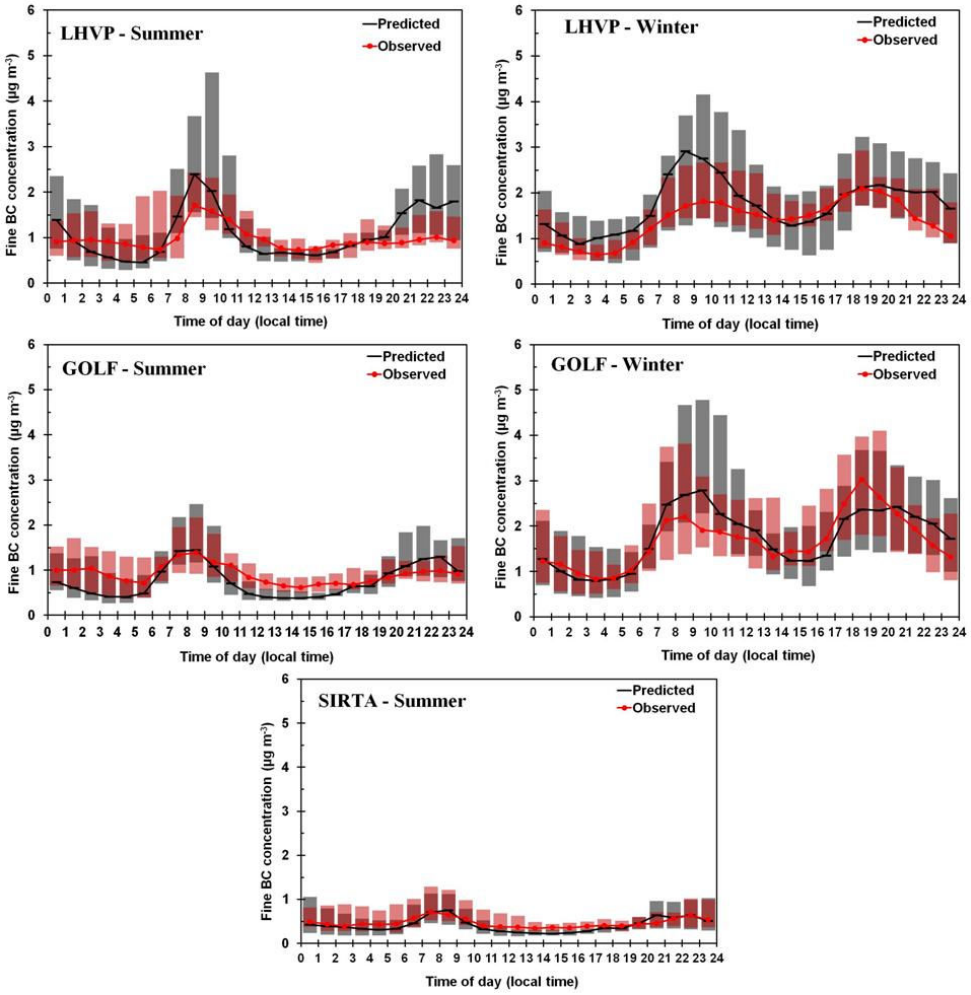

850

851 **Figure 6.** Average diurnal profiles of fine BC concentrations from the three measurement
852 stations during the MEGAPOLI summer and winter campaigns. The shaded vertical bars
853 indicate the 25th and 75th percentiles (gray color represents the predicted and pink the
854 observed values).

855

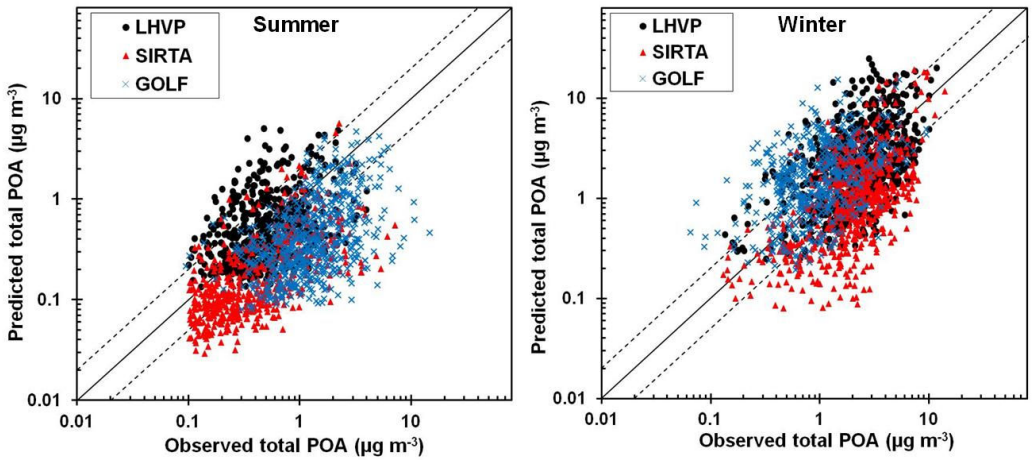

Figure 7. Comparison of predicted vs. observed PM_1 total POA (µg m^{-3}), including the added COA emissions, from the three measurement stations during the MEGAPOLI summer and winter campaigns. Each point is an hourly average value. Also shown are the 1:1, 2:1 and 1:2 lines. Observed data represent AMS factor-analysis results.

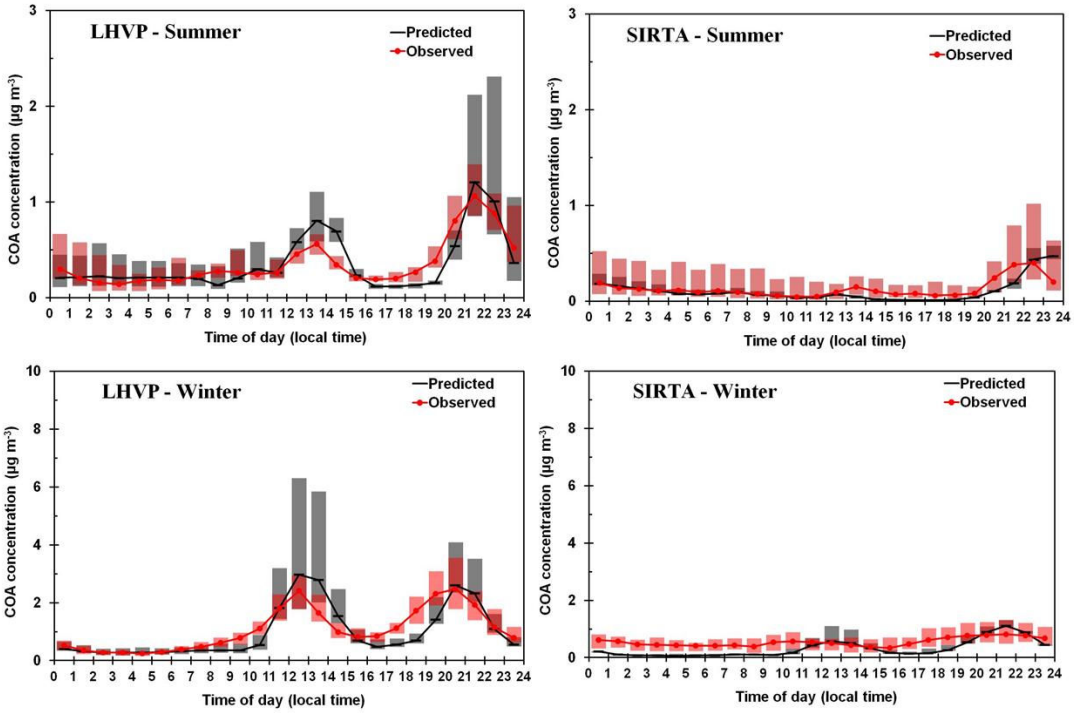

Figure 8. Average diurnal profile of COA concentrations in LHVP and SIRTA during the MEGAPOLI summer and winter campaigns. The shaded vertical bars indicate the 25th and 75th percentiles (gray color represents the predicted and pink the observed values).